Growth and characterization of ZnO multipods on functional surfaces with different sizes and shapes of Ag particles*

A Kamalianfar[a)b)], S A Halim[a)c)†], Mahmoud Godarz Naseri[d)], M Navasery[a)], Fasih Ud Din[a)], J A M Zahedi[e)], Kasra Behzad[f)], K P Lim[a)], A Lavari Monghadam[b)], and S K Chen[a)]

[a)] *Department of Physics, Faculty of Science, University Putra Malaysia, 43400 UPM Serdang, Selangor, Malaysia*
[b)] *Department of Physics, Farhangian University, Iran*
[c)] *Institute for Mathematical Research, University Putra Malaysia, 43400 UPM Serdang, Selangor, Malaysia*
[d)] *Department of Physics, Faculty of Science, Malayer University, Malayer, Iran*
[e)] *Department of Physics, Karaj Branch, Islamic Azad University, Karaj, Iran*
[f)] *Department of Physics, Science Faculty, Shahr-e-Ghods Branch, Islamic Azad University, Tehran, Iran*

(Received 1 December 2012; revised manuscript received 7 January 2013)

Three-dimensional ZnO multipods are successfully synthesized on functional substrates using the vapor transport method in a quartz tube. The functional surfaces, which include two different distributions of Ag nanoparticles and a layer of commercial Ag nanowires, are coated onto silicon substrates before the growth of ZnO nanostructures. The structures and morphologies of the ZnO/Ag heterostructures are investigated using X-ray diffraction and field emission scanning electron microscopy. The sizes and shapes of the Ag particles affect the growth rates and initial nucleations of the ZnO structures, resulting in different numbers and shapes of multipods. They also influence the orientation and growth quality of the rods. The optical properties are studied by photoluminescence, UV-vis, and Raman spectroscopy. The results indicate that the surface plasmon resonance strongly depends on the sizes and shapes of the Ag particles.

Keywords: ZnO, ZnO–Ag, surface plasmon resonance

PACS: 81.10.Bk, 79.60.Jv, 78.68.+m **DOI:** 10.1088/1674-1056/22/8/088103

1. Introduction

During the past few decades, a significant step after the growth of single-component nanostructures was to synthesize the heterostructure nanocrystals of materials. The study of metal interfaces in metal–semiconductor heterostructure nanocrystal systems has been of great interest in improving optical properties such as luminescence intensity and enhancing the efficiencies of light-emitting materials.[1–5] Additionally, the interaction between the components can produce new physical properties, which may be of great utilization in electronic and optoelectronic devices.

One of the most widely investigated semiconductor materials, ZnO, has a wide direct band gap ($E_g = 3.37$ eV) and high excitation energy (~ 60 meV) at room temperature, making it a promising candidate for optoelectronic devices.[6] To date, much attention has been paid to the synthesis of one- or two-dimensional ZnO nanostructures comprising belts, wires, rods, sheets, and walls.[7–11] Among them, some novel morphologies based on micro or nanostructures in three dimensions have attracted much attention due to their large volume-to-surface ratios.[12–14]

A functional surface means a surface that is modified (e.g. a metal-coated surface) to provide an improved function in a composite. Once light with a wavelength larger than the particle size of a metal strikes the surface of the metal, the resonance condition causes the free electrons in the metal to oscillate. This is referred to as the surface plasmon resonance. The size and shape variation of the nanoparticles can affect the oscillation frequency of the electrons and change the absorption and scattering of the light. This means that the optical properties of metal–semiconductor heterostructures depend on the shapes and sizes of both the metal and the surrounding semiconductors.

Among all metals, noble metals such as gold and silver with wide surface plasmon and electron storage have been used to enhance the charge separation in metal–semiconductor systems.[15,16] Many studies of the surface-enhanced Raman scattering substrate[17,18] and photocatalysis of Ag/ZnO nanocomposites have been conducted.[19]

In the present work, we study the effects of the size and shape of Ag particles on the morphological and optical properties of ZnO/Ag heterostructures. We use commercial Ag nanowires (NWs) and two different distributions of Ag nanoparticles (NPs) coated on silicon substrates. A simple and cost-effective approach, the vapor phase transport method, is employed to grow the ZnO nanostructures. As a point of reference, clean silicon is also chosen. The products are characterized and the relevant growth mechanism is proposed.

*Project supported by the Exploratory Research Grant (ERGS) (Grant No. ERGS//11/STG/UPM/01/3).
†Corresponding author. E-mail: ahalim@science.upm.edu.my
© 2013 Chinese Physical Society and IOP Publishing Ltd

2. Experiment

The substrates used in this study were silicon (1 1 1), and were cleaned with acetone and ethanol in a bath for 30 min. Two different distributions of Ag NPs were deposited on the substrates using physical vapor deposition (PVD). Using a spin coating method, commercial Ag NWs, each several hundred nanometers in length and about 50 nm–70 nm in diameter, were coated onto another silicon substrate. Pre-annealing was applied to the substrates at 700 °C for 30 min for good adherence to the surfaces. The experiment was carried out in a quartz tube using the vapor phase transport of a carbon–zinc oxide mixture at 950 °C. The setup was composed of a horizontal electric tube furnace (100 cm in length and 5 cm in diameter), a closed-end quartz tube (50 cm in length and 2 cm in diameter), a gas supply system, and two alumina boats. A mixture of zinc oxide (99.99%) and commercial graphite powder (1:1 weight rate) was loaded onto the alumina boat, which was inserted at the end of the quartz tube near the closed end. Another boat loaded with the substrates was placed downstream of the quartz tube, and the closed end of the quartz tube was inserted into the center of the horizontal electric tube.

The source was heated at a rate of 20 °C/min. When the temperature of the furnace reached 850 °C, nitrogen as the carrier gas was supplied to the furnace tube at a constant rate of 70 sccm. The temperature of the source was kept at 950 °C during 50 min of the growth process. Under these conditions, the temperature of the substrates was estimated to be approximately 750 °C. Finally, the electric furnace was cooled down to room temperature.

The products were characterized by field emission scanning electron microscopy [FESEM, JSM 6700] and an X-ray diffractometer [XRD, pw 3040 MPD]. The photoluminescence (PL) measurements were performed at room temperature using a fluorescence spectrometer (LS 55, Xe lamp). Absorption plots of the samples were obtained using ultraviolet-visible spectroscopy (UV-Vis 3600 SHIMADZU), and the Raman spectra of the samples were recorded using a Raman spectrometer (Renishaw inVia with $\lambda = 514$ nm laser excitation).

3. Results and discussion

Figure 1 shows the FESEM images of the pre-deposition Ag layers on the silicon substrates after annealing. Figure 1(a) shows a clean silicon that was used for reference. The quasi-spherical Ag particles with different densities and sizes are shown in Figs. 1(b) and 1(c). The Ag particles in sample A have an average diameter of about (130 ± 10) nm. Sample B has the larger Ag particles with an average diameter of about (310 ± 10) nm. As can be seen in Fig. 1(d), the commercial Ag NWs (with a base dimension of (200 nm–300 nm) $\times$ (800 nm–1000 nm) were adhered to each other and particles with non-spherical symmetries were formed on the substrates.

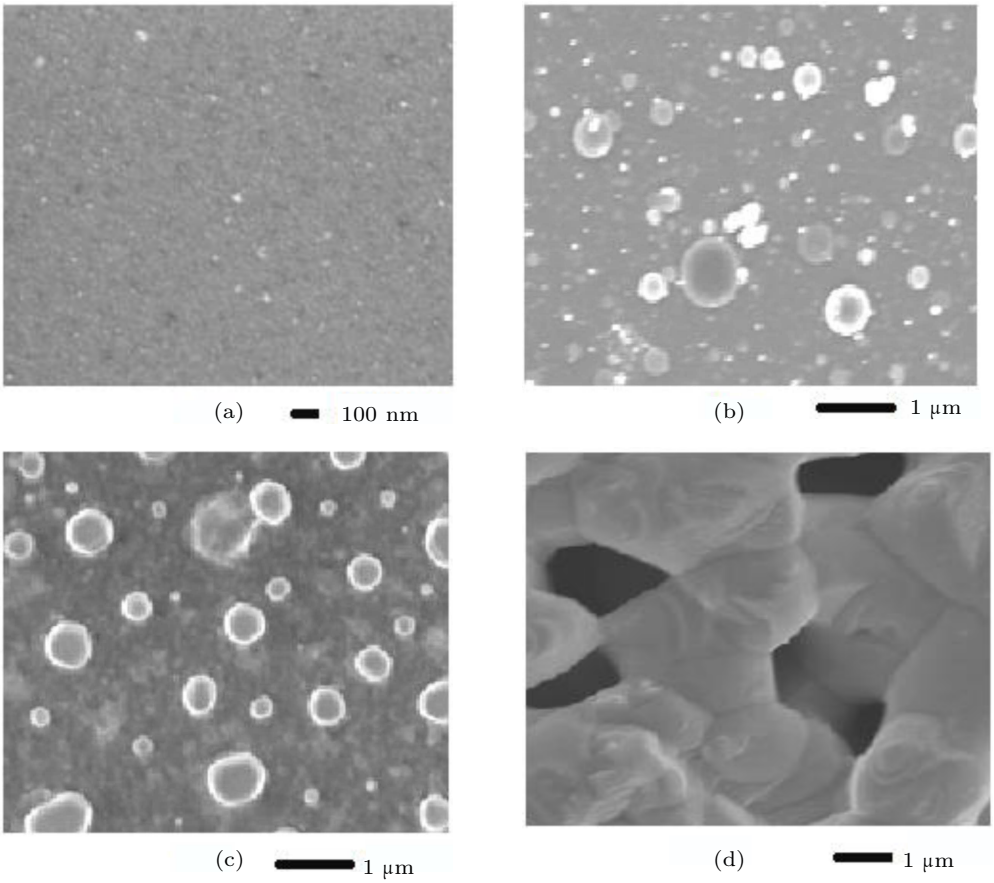


Fig. 1. The FESEM images of the substrates with pre-deposition Ag layers for (a) clean silicon, (b) a low distribution of Ag NPs, (c) a high distribution of Ag NPs, and (d) adhered Ag NWs.

The ZnO nanostructures grown on substrates with different sizes and shapes of Ag are shown in Fig. 2. It can be seen that the surfaces of the substrates are all covered with various ZnO nanostructures. As a point of reference, the morphology of the ZnO structure grown on a clean silicon substrate can be seen in Fig. 2(a). The surface of the clean silicon is covered with a layer of randomly oriented ZnO nanospears with an average diameter of about 150 nm. The lengths of the spears whose diameters gradually reduce down from 150 nm to 100 nm reach 10 μm (see the inset of Fig. 2(a)).

The multipods composed of nanowires and nanorods grow into different distributions of Ag NPs as shown in Figs. 2(b) and 2(c). The surfaces of samples A, B, and C exhibit multipod crystals consisting of a number of legs united at the same junction, several micrometers in length. Although, they display morphologies with a similar structure (multipods), the different distributions and shapes of the Ag particles strongly influence the sizes and orientations of the ZnO rods and wires.

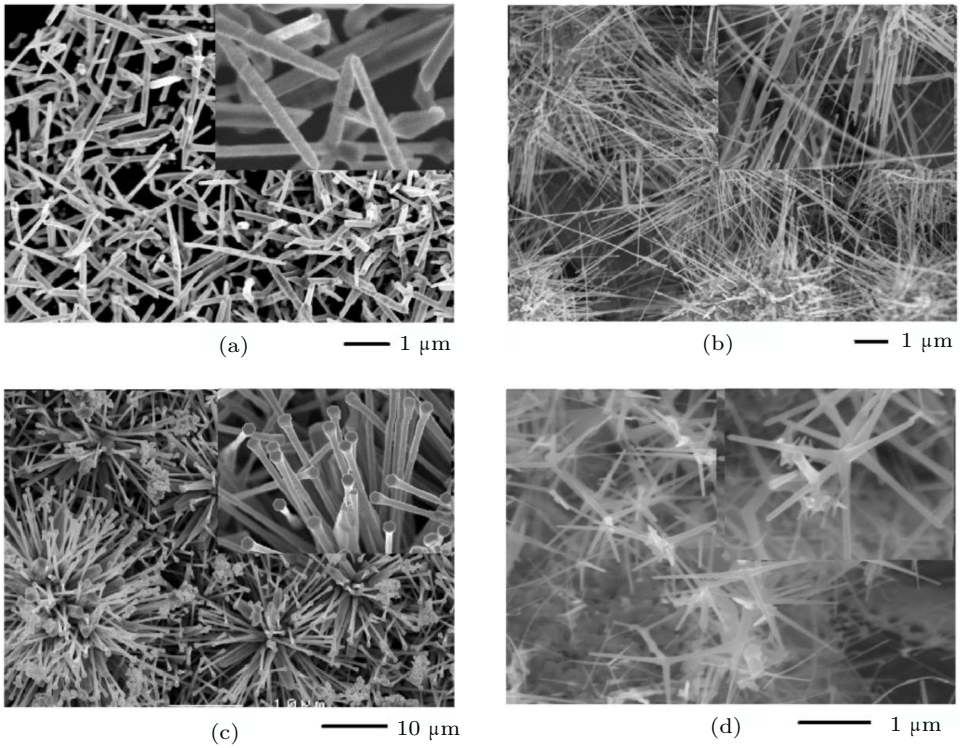


Fig. 2. FESEM images of ZnO nanostructure arrays with different pre-deposition Ag layers for (a) pure ZnO, (b) sample A, (c) sample B, and (d) sample C. The insets show high magnification images of the corresponding surfaces.

Figure 2(b) shows the FESEM image of sample A with a low distribution of Ag NPs. As shown in the figure, ZnO multiples consist of nanowires extended out of discontinuous ZnO nucleation islands and have a radial substrate growth direction. The wires have diameters ranging from 50 nm to 100 nm and lengths of several micrometers (see the inset of Fig. 2(b)).

Figure 2(c) presents the surface morphology of sample B. The surface is covered with multipod crystal composite nanorods 400 nm–500 nm in diameter and several micrometers in length. The pods present a hexagonal shape at their tips and tend to align quasi-vertically along the normal to the substrate. The surface morphology of sample C grown on a layer of adhering Ag NWs is shown in Fig. 2(d). The sample consists of multileg ZnO whiskers. It can be seen that each multileg consists of a tetrapod structure grown along the main arm. The length of the leg is less than 2 μm and the diameters of the legs are in the range 100 nm–150 nm.

The growth mechanism of the ZnO nanopod has been debatable up to now, but the growth mechanism of ZnO nanowires on a silicon surface without catalyst can be explained on the basis of the vapor–solid (VS) growth mechanism.[20] In addition, no Ag particles were detected at the top of nanowires by EDX, indicating that the VS mechanism is appropriate for explaining the growths of the sample A, B, and C structures. The reason why they can be explained is based on the higher supersaturation of Zn vapor. Rods and wires grow at high temperature with the vapor transport method (VPT) method. This means that the Zn vapor deposits at a fast rate. No reaction occurs between Zn vapor and the catalyst particles due to the shortage of time. A hypothetical model is shown in Fig. 3 to explain the formation of ZnO multipods. After the reaction of ZnO source material with carbon

in the high-temperature zone of the quartz tube, ZnO reduces into Zn, ZnO_x, and O_{1-x}. Then, gaseous Zn atoms transfer toward the substrate zone with lower temperature. The recombination of oxygen and Zn yields ZnO nanowires or nanorods. Some factors are important in forming a variety of structures. One is the supersaturation of vapor to obtain the desired morphology and nanostructure size.[21]

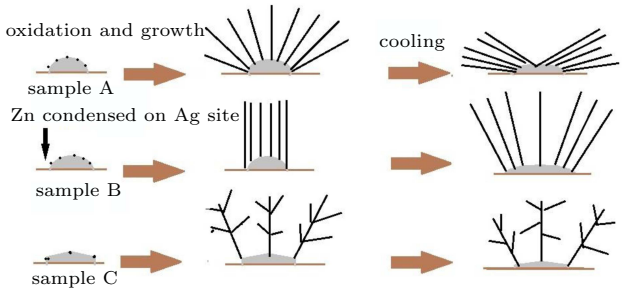


Fig. 3. (color online) Illustration of a hypothetical model for the growth of nanorods.

Iwanaga *et al.*[22] reported on a model to explain the formation of ZnO tetrapod structures. The first stage forms ZnO nuclei due to the reaction between gaseous Zn atoms and O atoms. In the next stage, some of the twin boundaries in the ZnO nuclei crack due to the deficiency of oxygen, and the final stage is to extend out of the arms of the emerged octahedral crystals.

Now, the question is what are the effects of the size and shape of the Ag particles on the formation of the multipod? The answer can be as follows. The number of legs grown from a unique junction can be assigned to the density of the Ag particles on the substrate. As is well known, the metal particles coated on the substrate adsorb the gaseous Zn atoms. Sample A has a low distribution of Ag particles. As a result, the number of gaseous Zn atoms that can be absorbed by the Ag sites are more than that in sample B. During cooling to room temperature, the Ag particles undergo a tensile or compressive stress due to the difference in the thermal expansion coefficient between the Ag particles and silicon substrate ($\alpha_{Ag} \cong 6\alpha_{si}$). The oxygen vacancies can also cause an internal stress. To relieve the stress, the Ag particles try to overspread on the substrate. This expansion affects the direction of the wire, as can be seen in the FESEM images of samples A and B.

The XRD patterns of the ZnO nanostructures are shown in Fig. 4. The observed diffraction peaks in the patterns can be divided into two parts. The main part can be indexed to the hexagonal ZnO structure (JCPDS card, No. 36-1451, $a = 3.249$ Å, $c = 5.206$ Å). The peaks at 38.2°, 44.4°, and 64.6° can be indexed to face-centred-cubic metallic Ag (JCPDS card, No, 04-0783), suggesting that the products are ZnO/Ag composites.

As can be seen in the Ag XRD peaks, the intensity of the Ag (1 1 1) peak is higher than that of the other peaks, indicating that most of the Ag islands are enclosed with the (1 1 1) plane. In the case of sample C, the peaks corresponding to the undercoating Ag NWs are much more intense than those of samples A and B, indicating the contribution of the undercoating Ag NWs in the composite.

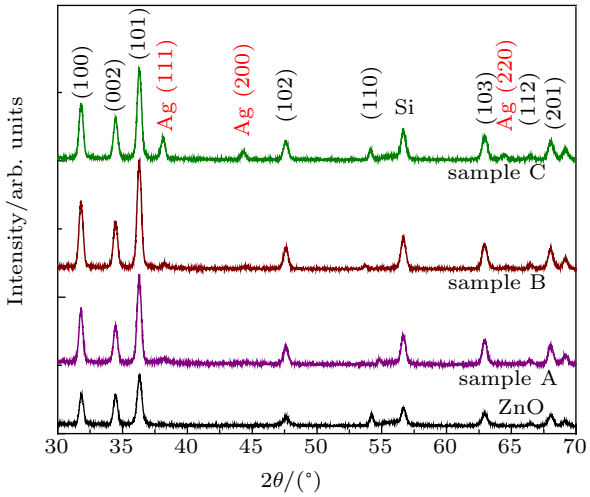


Fig. 4. (color online) The XRD patterns of the pure ZnO and ZnO/Ag nanocomposites.

4. Optical properties

4.1. Photoluminescence spectroscopy

To study the optical properties of the prepared samples, PL measurements were performed at room temperature with an excitation wavelength of 320 nm. Figure 5 shows the PL spectra of the samples and pure ZnO nanostructures. For the pure ZnO, a weak UV peak centred at 384 nm and a dominant and broad visible emission peak centred at 490 nm were observed. It is supposed that the UV emission, called the near band edge emission, arises from the recombination of free excitons through an exciton–exciton collision process,[23] and the broad visible emission is due to the presence of various types of defect.[24,25]

A dominant and sharp UV emission peak in the range 380 nm–383 nm was observed for the samples with a predeposited Ag nanostructure. They exhibited a much weaker deep level emission at 490 nm. The decrease in UV emissions for samples A, B, and C may be caused by the electron trapping effect of silver, and named the reduction of zinc oxide photocatalytic activity.[26] A possible quenching effect on the light emission of zinc oxide in the visible region due to the charge transfer between Ag and ZnO cannot be ruled out[27] (see the next subsection about UV-vis). Since the specific nanostructure may show the specific defect, one might expect that the recombination of a singly ionized charge state of this defect and a photogenerated hole is responsible for this irregular behavior.[28] As noted earlier, the average size and density of Ag particles in sample B are more than in sample A, but the intensity of the UV emission for sample A is more than that for

samples B and C. The reason for this can be found in the size and shape of Ag particles. Sample A has the smallest average size of Ag particles in samples A, B, and C. When a light beam is incident on the Ag surface, the electrons of the Ag atoms are caused to oscillate with the frequency of the light, resulting in separation of the metal core from the electron cloud of the Ag particles. This separation of charges also produces the electron–hole pairs within the semiconductor particles. Consequently, the Ag particle acts as an electron sink and prohibits the recombination of photoinduced electrons and holes. This means that the number of metal sites that prohibit the recombination of electrons and holes in sample A is less than that in samples B and C. As is well known, UV emission (the near band edge emission) arises from the recombination of free excitons, and as a result, the PL intensity of the Ag/ZnO structure decreases with the increase in Ag particle size.

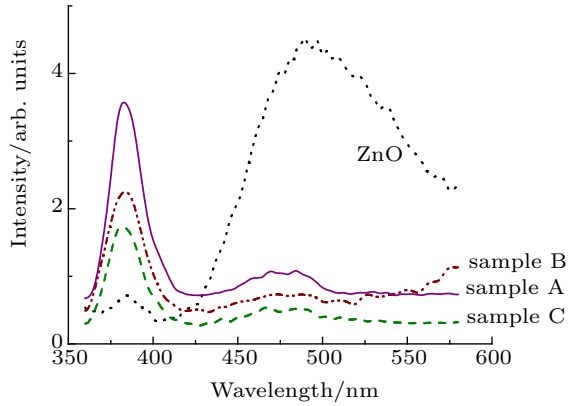


Fig. 5. (color online) The PL spectra of the pure ZnO and ZnO/Ag nanocomposites.

4.2. The UV-vis spectrum

The optical absorption spectra of samples A, B, C, and pure ZnO are presented in Fig. 6. As can be seen in the spectra, the absorption of pure ZnO exhibits UV absorption at 345 nm. This can be referred to as the exciton absorption peak of ZnO nanospears. By introducing Ag particles with spherical symmetry, only one dipolar plasmon resonance appears, under which all the particles between the negative and positive poles are excited due to the free electrons and lattice, respectively. The shoulder centred in a 400 nm–420 nm range for samples A, B, and C is called the localized surface plasmon resonance of ZnO–Ag nanocomposites. Comparing the plots of samples A and B, the absorption of the surface plasmon exhibits a slight red-shift with the distribution of Ag nanoparticles on the substrate increasing. This red-shift may be caused by the strong interfacial coupling between Ag nanoparticles.

When the sizes of Ag particles change or their shapes become more complex, the number of nondegenerate dipolar modes rises. As a result, their optical absorption plots show some bands over a broad spectral region. In the case of sample C with nonspherical Ag particles, the induced electronic cloud is not distributed homogeneously on the functional surface and the distribution of charges is multipolar. As a result, dipolar modes with different resonant frequencies appear on the surface.

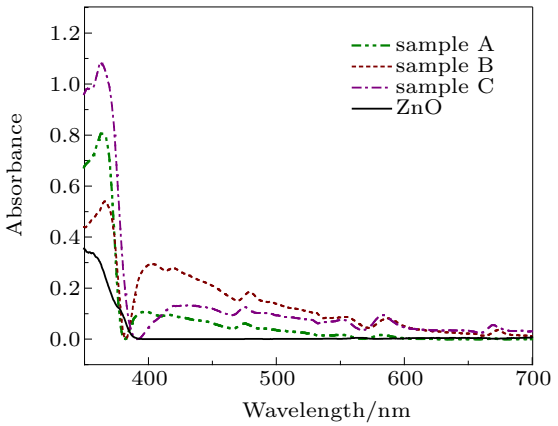


Fig. 6. (color online) The UV-vis absorption spectra of the synthesized samples.

The position of the plasmon absorption of a metal can be calculated by the following equation:[29]

$$\lambda_{\mathrm{p}} = \left[4\pi^2 c^2 m_{\mathrm{eff}} \epsilon_0 / N e^2\right]^{1/2}. \quad (1)$$

In this equation, the effective mass and electron density are denoted by m_{eff} and N, respectively. So small red-shifts at the plasmon absorption positions of samples B and C indicate that the electron density of Ag is reduced. The reduction in silver electron density can be explained by referring to the Fermi energy levels of ZnO and Ag, as presented in Fig. 7. The work function of ZnO (4.3 eV) is larger than that of Ag (4.1 eV), and therefore ZnO has a lower Fermi level than silver. As a result, electrons can transfer from Ag to ZnO nanostructures while the two systems are not in equilibration. So, a change in the electron density may be described by the transfer of electrons from the Ag to ZnO matrix.

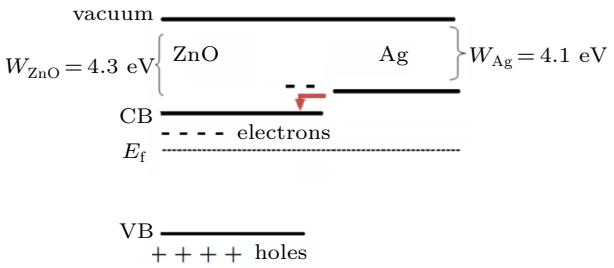


Fig. 7. (color online) Illustration of the energy level of ZnO–Ag.

4.3. The Raman spectrum

Raman scattering spectroscopy is a technique based on the change in frequency of photons that takes place when a monochromic light interacts with a specimen. It provides information about the chemicals, crystal perfection, and structural defection. Additionally, the vibrational modes are important factors for investigating the thermal and electrical prop-

erties of a single crystal, such as the wurtzite ZnO structure based on its low and high field carrier transport. There are $3P$ branches for a lattice with P atoms per unit cell. So, ZnO with four atoms per unit cell (two Zn–O molecular units) has 12 phonon modes, of which three are acoustic, i.e., one longitudinal-acoustic (LA) mode and two transverse-acoustic (TA) modes, and the $3P-3=9$ branches are optical, i.e., three longitudinal-optical (LO) modes and six transverse-optical (TO) modes. Based on the group theory prediction, near the zone-center there is an A1 branch and a twofold degenerate $E1$ branch, which are Raman and infrared-active split into LO and TO modes. There are also two twofold degenerate $E2$ branches that are Raman-active.[30]

Figure 8 shows the characteristic Raman features of the samples and pure ZnO at room temperature. In the case of pure ZnO, a sharp and dominant mode at 436.7 cm^{-1} is observed. For the Ag–ZnO nanocomposites, this peak is located at 435.4 cm^{-1}. The shift in the $E2$ phonon frequency toward higher frequencies (shorter wavelength) is due to a compressive stress, whereas a decrease in the frequency of the $E2$ mode is because of a tensile stress.[31] The $E2$ phonon frequencies for pure ZnO, samples A, B, and C, are measured to be 436.65, 437.84, 435.45, and 434.27 cm^{-1}, respectively. These values indicate that the pure ZnO thin film has an $E2$ mode similar to the standard bulk (437 cm^{-1}). Sample A, with a low distribution of spherical Ag particles, shows a 1.2 cm^{-1} shift toward the higher frequency, which can be attributed to the case due to compressive stress. On the contrary, samples B and C present a 1 cm^{-1} and 2.4 cm^{-1} shift toward lower frequency, respectively. Thus, atensile stress occurs separately in samples B and C. The stresses can originate from an oxygen vacancy or difference in thermal expansion coefficient between the components.

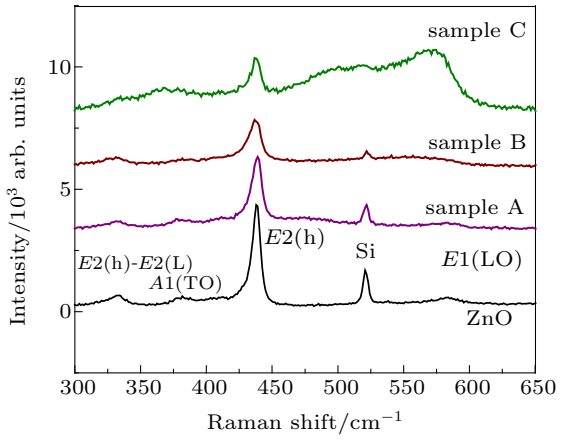


Fig. 8. Raman spectra excited by a 514 nm line of the synthesized samples.

A very suppressed and weak peak at 585 cm^{-1}, attributed to the $E1$ (LO) mode, appears. It is generally considered that the $E1$ (LO) mode produces the peak due to the formation of defects (oxygen vacancies or zinc interstitials).[32] From the comparative intensity of $E1$ (L), it is clear that the intensity of $E1$ (LO) is reduced by introducing Ag nanostructures between ZnO and the silicon substrate. This means that the crystal perfectness of samples B and C is better than that of sample A. Some other peaks at 332, 380, and 531 cm^{-1} are also observed in the spectrum assigned to the ($E2$ (h)–$E2$ (l)) (multi phonon), $A1$ (T), $E1$ (T), and $E2$ (LA) modes, respectively.

5. Conclusions

The structural and optical properties of ZnO/Ag multipods, which are dependent on the sizes and shapes of the Ag nanostructures, are investigated. The FESEM results indicate that the multipods composed of nanorods in the sample with a distribution of more Ag particles tend to align vertically. The functional surface with Ag particles enhances the absorption of visible light, which is attributed to surface plasmon resonance. The enhancement of the UV emission can be ascribed to the surface plasmon resonance, which causes the Ag particles to act as an electron sink and prohibits the recombination of photoinduced electrons and holes. When Ag NWs are used instead of NPs, the number of non-degenerate dipole modes increases due to the asymmetrical shapes, resulting in the occurrence of dipole modes with different resonant frequencies. So the optical absorption plot shows some bands over a broad spectral region. The changes in the optical properties of ZnO using functional surfaces will have many applications in plasmonics, optics, electro-optics devices, and photocatalysis.

References

[1] Biteen J S, Pacifici D, Lewis N S and Atwater H A 2005 *Nano Lett.* **5** 1768
[2] Hsieh Y P, Liang C T, Chen Y F, Lai C W and Chou P T 2007 *Nanotechnology* **18** 415707
[3] Lin H Y, Cheng C L, Chou Y Y, Huang L L and Chen Y F 2006 *Opt. Express* **14** 2372
[4] Lai C W, An J and Ong H C 2005 *Appl. Phys. Lett.* **86** 251105
[5] Kamalianfar A, Halim S A, Kasra Behzad, and Mahmoud Goodarz Naseri 2013 *J. Optoelectron. Adv. Mater.* **15** 239
[6] Zhao J W, Liu F J, Huang H Q, Hu Z F and Zhang X Q 2012 *Chin. Phys. B* **21** 065201
[7] Wang Z L 2009 *Mater. Sci. Eng. R* **64** 33
[8] Hsueh T J, Hsu C L, Chang S J and Chen I C 2007 *Sensor Acttuat. B: Chem.* **126** 473
[9] Yi G C, Wang C and Park W I 2005 *Semicond. Sci. Technol.* **20** S22
[10] Xiao Q, Huang S, Zhang J, Xiao C and Tan X 2008 *J. Alloys Compd.* **459** L18
[11] Su S C, Lu Y M, Zhang Z Z, Li B H, Shen D Z, Yao B and Zhang J Y 2008 *Physica B* **403** 2590
[12] Mishra P, Yadav R S and Pandey A C 2010 *Ultrason. Sonochem.* **17** 560
[13] Kamalianfar A, Halim S A, Pilban Jahromi S and Navasery M 2012 *Chin. Phys. Lett.* **29** 128102
[14] Zhang Z L, Zheng G, Qu F Y and Wu X 2012 *Chin. Phys. B* **21** 098104
[15] Merga G, Cass L C, Chipman D M and Meisel D 2008 *J. Am. Chem. Soc.* **130** 7067
[16] Li C, Fang G J, Guan W J and Zhao X Z 2007 *Mater. Lett.* **61** 3310
[17] Deng S, Fan H M, Zhang X, Loh K P, Cheng C L, Sow C H and Foo Y L 2009 *Nanotechnology* **20** 175705
[18] Schmidt J P, Cross S E and Buratto S K 2004 *J. Chem. Phys.* **121** 10657

[19] Wang J, Fan X M, Tian K, Zhou Z W and Wang Y 2011 *Appl. Surf. Sci.* **257** 7763
[20] Zheng W P, Wau Z, Dai Z R and Wang Z I 2001 *Science* **291** 1947
[21] Yousefi R and Kamaluddin B 2009 *J. Alloys Compd.* **479** L11
[22] Iwanaga H, Fujii M and Takeuchi S 1993 *J. Crystal Growth* **134** 275
[23] Fonoberov V A, Alim K A, Balandin A A, Xiu F and Liu J 2006 *Phys. Rev. B* **73** 165317
[24] Fonoberov V A and Balandin A A 2004 *Appl. Phys. Lett.* **85** 5971
[25] Dingle R 1969 *Phys. Rev. Lett.* **23** 579
[26] Lu W W, Gao S Y and Wang J J 2008 *J. Phys. Chem. C* **112** 16792
[27] Yin X, Que W, Fei D, Shen F and Guo Q 2012 *J. Alloys Compd.* **524** 13
[28] Vanheusden K, Warren W L, Seager C H and Tallant D R 1996 *J. Appl. Phys.* **79** 7983
[29] Shan G, Xu L H, Wang G R and Liu Y 2007 *J. Phys. Chem. C* **111** 3290
[30] Rajalakshmi M, Akhilesh K A, Bendre B S and Shailaja Mahamuni 2000 *Appl. Phys. Lett.* **87** 2445
[31] Damen T C, Porto S P S and Tell B 1966 *Phys. Rev.* **142** 570
[32] Wang X, Li Q, Liu Z and Zhang J 2004 *Appl. Phys. Lett.* **84** 4941